A Kirkwood−Buff Derived Force Field for Thiols, Sulfides, and Disulfides

Nikolaos Bentenitis,[†] Nicholas R. Cox,[†] and Paul E. Smith*[,‡]

Department of Chemistry and Biochemistry, Southwestern University, Georgetown, Texas 78626, and Department of Chemistry, Kansas State University, Manhattan, Kansas 66506

Received: May 22, 2009; Revised Manuscript Received: July 22, 2009

A force field has been developed for molecular simulations of methanethiol, dimethyl sulfide, and dimethyl disulfide mixtures. The force field specifically attempts to balance the solvation and self-association of these solutes in solution mixtures with methanol. The force field is based on the Kirkwood−Buff (KB) theory of solutions and is parametrized using the KB integrals obtained from the experimental activity coefficients for the solution mixtures. The transferability of the force field was tested and confirmed by the accurate prediction of the activity coefficients for methanethiol/dimethyl sulfide solutions, which were not used in the initial parametrization of the force fields. The ideality of this latter solution is excellently reproduced. The applicability of the force field to simulations in water was corroborated with a reasonably accurate prediction for the low solubility of dimethyl sulfide in water. The aggregation of methanol molecules at low methanol mole fractions displayed by all the mixtures is reproduced and further analyzed.

Introduction

Improved peptide and protein force fields are important for the accurate simulation of many biological systems. Current force fields are usually developed using parameters for molecules which represent the typical functional groups observed in amino acids.[1−4] The quality of the results obtained using such a force field then depends on the accuracy of the interactions between different functional groups and between the functional groups and the solvent of interest (usually water). Recently, we have been describing models which can eventually be used to develop a peptide and protein force field that accurately reproduces the correct balance between solvation and self-association of model solute molecules in solution.[5−10] The approach is based on the Kirkwood−Buff (KB) theory of solutions, a theory that relates the microscopic solution structure, which can be obtained by molecular simulation, to the thermodynamic properties of solutions, as obtained by experiment.[11,12] At present, we have developed a Kirkwood−Buff derived force field (KBFF) for methanol (MOH, a model for serine),[6] trans *N*-methylacetamide (a model for the peptide group),[5] *N*,*N*-dimethylamide (a model for proline),[5] and acetamide (a model for asparagine and glutamine).[5] Here, we extend the previous studies to provide force fields for methanethiol (MSH, a model for cysteine), dimethyl sulfide (MSM, a model for methionine), and dimethyl disulfide (DDS, a model for disulfide bonds).

Our basic approach to force field development was recently described in detail.[13] Other researchers have also explored similar ideas.[14,15] Briefly, the KBFF approach aims to accurately predict the thermodynamic properties of solution mixtures, in particular the excess Gibbs free energy and the excess enthalpy of the solution. To achieve this goal we have focused on fine tuning the effective charge distributions for solutes in polar solvents, without including explicit polarization terms. While we focus on thermodynamic properties of solution mixtures to parametrize our force field, the KBFF models also generally reproduce the physical and thermodynamic properties of the pure substances and the physical properties of both pure liquids and solution mixtures.

The solvent used in this work is methanol, and not water, which was used in the development of our previous force fields. Methanol has been used because MSH, MSM, and DDS are only sparingly soluble in water but completely miscible in methanol. Therefore, experimental activity coefficients in water are rather limited, whereas those in methanol are available.[16,17] Since we have already presented a force field for methanol,[6] our working assumption is that the force field parameters for MSH, MOH, and MSM determined by studying mixtures with methanol will be transferable to aqueous solutions. A preliminary test of this assumption was performed by determining the solubility of MSM in SPC/E[18] water after the parametrization was complete.

It should be noted that there are two force fields specific for MSH, MSM, and DDS that can be found in the literature: one by Delhommelle et al.[19] and one by Lubna et al.[20] The parameters for both of these force fields were optimized to reproduce experimental vapor−liquid equilibria data for the pure substances as a function of temperature. The authors did not study in detail the thermodynamics of mixtures of these solutes with methanol or any other solvents. Unfortunately, as shown in the Results section, our force field for methanol is incompatible with either of the two existing force fields, in that one cannot reproduce the experimentally obtained KB integrals for the solution mixtures. Futhermore, we have previously shown that common force fields available in the literature usually perform poorly in their ability to reproduce the experimental KB integrals.[5,10] Consequently, we have decided to develop our own force fields for MSH, MSM, and MSM that provide an accurate balance between solute solvation and solute self-association in these systems. In addition, we investigate a variety of other properties of the solutions not available experimentally including: self-diffusion constants, enthalpy of mixing, the extent of hydrogen bonding, and degree of molecular aggregation.

* Corresponding author. Department of Chemistry, 213 CBC Building, Kansas State University, Manhattan, KS 66506-0401. Tel.: 785-532-5109. Fax: 785-532-6666. E-mail: pesmith@ksu.edu.
[†] Southwestern University.
[‡] Kansas State University.

10.1021/jp904806f CCC: $40.75
Published on Web 08/14/2009

Methods

Kirkwood−Buff Analysis of the Experimental Data. The experimental data for all binary mixtures were analyzed according to the procedure described by Ben-Naim.[11,21,22] Using KB theory, a series of thermodynamic properties of solution mixtures can be related to the solution distributions through the KB integrals, G_{ij}, defined as

$$G_{ij} = 4\pi \int_0^\infty [g_{ij}^{\mu VT}(r) - 1] r^2 \mathrm{d}r \quad (1)$$

where $g_{ij}^{\mu VT}$ is the radial distribution function between molecules i and j in the μVT ensemble. For a binary mixture of a solute (2) and a solvent (1), one can define excess coordination numbers, $N_{ij} = \rho_i G_{ij}$, which are related to the experimental data according to the following expressions

$$N_{11} = \rho_1 RT\kappa_T - 1 + \frac{\rho_2 \bar{V}_2^2 \rho}{D} \quad (2)$$

$$N_{22} = \rho_2 RT\kappa_T - 1 + \frac{\rho_1 \bar{V}_1^2 \rho}{D} \quad (3)$$

$$N_{12} = \rho_2 RT\kappa_T - \frac{\rho_2 \bar{V}_1 \bar{V}_2 \rho}{D} \quad (4)$$

where R is the gas constant; T is the solution temperature; $\rho_i = x_i/V_\mathrm{m}$ is the number density of component i; x_i is the mole fraction of component i; V_m is the molar volume of the solution; $\bar{V}_i$ is the partial molar volume of component i; κ_T is the isothermal compressibility of the solution, $\rho = 1/V_\mathrm{m}$ and

$$D = \frac{x_1}{RT}\left(\frac{\partial \mu_1}{\partial x_1}\right)_{T,P} = \left(\frac{\mathrm{d} \ln \gamma_1}{\mathrm{d} \ln x_1}\right)_{T,P} + 1 \quad (5)$$

where $\mu_i = \mu_i^\circ + RT \ln(x_i\gamma_i)$ is the chemical potential of component (1) using the mole fraction concentration scale with the pure component as the standard state and γ_1 is the activity coefficient of component (1).

The chemical potential derivative, D, is determined from the experimentally observed activity coefficients. More specifically, for the MSH/MOH and MSM/MOH solutions the experimental activity data from Jackowski,[16] provided in terms of the Wilson equation[23]

$$\ln \gamma_1 = -\ln(x_1 + \Lambda_{12}x_2) + x_2\left[\frac{\Lambda_{12}}{x_1 + \Lambda_{12}x_2} - \frac{\Lambda_{21}}{x_2 + \Lambda_{21}x_1}\right] \quad (6)$$

$$\ln \gamma_2 = -\ln(x_2 + \Lambda_{21}x_1) - x_1\left[\frac{\Lambda_{12}}{x_1 + \Lambda_{12}x_2} - \frac{\Lambda_{21}}{x_2 + \Lambda_{21}x_1}\right] \quad (7)$$

were used. Here, Λ_{12} and Λ_{21} are fitting constants. For consistency, the activity data provided by Jackowski[16] for MSH/MSM mixtures represented in terms of the Redlich−Kister equation were used to obtain equivalent Wilson equation parameters using regression. The choice of fitting equation used did not significantly affect the KB integrals extracted from the experimental data. Finally, the experimental data from Zudkewitch[17] for DDS/MOH mixtures were also used to obtain Wilson equation parameters by regression. Table 1 shows the experimental values of Λ_{12} and Λ_{21} for all systems that were used in this work.

TABLE 1: Fitting Parameters for the Wilson Equation

		Λ_{12}		Λ_{21}	
solution	T/K	experiment	simulation	experiment	simulation
MSH/MOH[a]	288	0.5576	0.8580	0.1101	0.2342
MSM/MOH[a]	288	0.4217	0.4787	0.1719	0.2172
MSH/MSM[a]	288	0.9624	0.8634	1.119	1.201
DDS/MOH[b]	311	0.2780	0.4155	0.2030	0.1801

[a] Experimental data from Jackowski.[16] [b] Experimental data from Zudkevitch et al.[17]

There were no available experimental data for the density or partial molar volumes of the solution components as a function of composition. However, variations in the partial molar volumes have only a small effect on the Kirkwood−Buff integrals.[24] Therefore, it was assumed that the partial molar volume, $\bar{V}_i$, of each component was constant and equal to the molar volume of the pure substance, V_i, for which values were taken from the literature.[25] Hence, we assumed that $V_\mathrm{m} = x_1\bar{V}_1 + x_2\bar{V}_2 = x_1V_1 + x_2V_2$. In addition, the KB integrals are also insensitive to the isothermal compressibility, κ_T, of the solution.[24] Hence, the latter was calculated according to the expression

$$\kappa_T = \varphi_1\kappa_{T,1} + \varphi_2\kappa_{T,2} \quad (8)$$

where $\varphi_i = \rho_i\bar{V}_i$ is the volume fraction of component i in solution and $\kappa_{T,i}$ is the isothermal compressibility of the pure substance i. Because the experimental isothermal compressibilities of MSH, MSM, and DDS were not available, we initially set the isothermal compressibility of the solution equal to that of MOH and calculated the experimental excess coordination numbers. We then calculated the isothermal compressibilities of MSH, MSM, and DDS from our simulations, recalculated the experimental excess coordination numbers, and found that they were almost identical to those calculated initially. This was expected because, as mentioned above, the KB integrals are insensitive to the isothermal compressibility of the solution.[24]

Molecular Dynamics Simulations. All mixtures were simulated via classical molecular dynamics techniques using the Gromacs program (version 3.3).[26] The simulations were performed in the isothermal−isobaric NpT ensemble at 1 atm and 288 K for the MSH/MOH, MSM/MOH, and MSM/MSH solutions and at 1 atm and 311 K for the DDS/MOH solutions. The Berendsen thermostat was used to modulate the temperature with a relaxation time of 0.1 ps, and the Berendsen barostat was used to modulate the pressure with a relaxation time of 0.5 ps. All bonds were constrained using the LINCS algorithm.[27] A 2 fs time step was used for integration of the equations of motion. The electrostatic interactions were evaluated using the particle-mesh-Ewald technique.[28] Cutoff distances of 1.0 nm and of 1.5 nm were used for the real space electrostatic and van der Waals interactions, respectively.

The number of molecules used for the simulation of the solution mixtures and the pure liquids are shown in Table 2. The number of molecules was chosen so that, based on the experimental density of the pure components, a cubic simulation box of approximately 1000 nm^3 was generated. Random initial configurations were generated, and the steepest descent method

TABLE 2: Summary of the MSH/MOH, MSM/MOH, MSH/MSM, and DDS/MOH Simulations[a]

	MSH/MOH		MSM/MOH		MSH/MSM		DDS/MOH	
	288 K		288 K		288 K		311 K	
X	N_{MSH}	N_{MOH}	N_{MSM}	N_{MOH}	N_{MSH}	N_{MSM}	N_{DDS}	N_{MOH}
0.0	0	1739	0	1739	0	1000	0	1739
0.125	1629	11413	1537	10769	1056	7400	1428	10013
0.250	3168	9507	2844	8533	2192	6576	2520	7565
0.375	4630	4630	3978	6631	3412	5687	3416	5694
0.500	6025	6025	4982	4982	4725	4725	4188	4188
0.625	7364	4418	5883	3530	6141	3684	4876	2925
0.750	8655	2885	6705	2235	7669	2556	5506	1835
0.875	9903	1414	7461	1065	9322	1331	6092	870
1.0	1329	0	1000	0	0	1329	0	1000

[a] All simulations were performed at 1 bar in cubic boxes of length ≈10 nm.

was used to perform 10 000 energy minimization steps. Equilibration runs of 200 ps followed to ensure that the total potential energy displayed no drift with time. Production runs of 10 ns were then performed and the velocities and configurations saved every 0.1 ps for analysis. The first 2.5 ns of the runs was discarded during the analysis.

Using utility programs within Gromacs, the self-diffusion constants, D_t, were determined from the mean square fluctuations, and the relative permittivities, ε, were calculated from the dipole moment correlation functions. For pure substances, shear viscosities, η, were calculated from the autocorrelation functions,[29] the isothermal compressibilities, κ_T, by performing additional simulations of 500 ps at 500 and 1000 atm, and heat capacities, C_P, and thermal expansion coefficients, α, by additional 500 ps simulations at 278 and 298 K for MSH and MSM and at 301 and 311 K for DDS. The excess enthalpies of mixing, ΔH^E_{mix}, were calculated from the average potential energies according to

$$\Delta H^E_{mix} = H_{sol} - x_1 H_1 - x_2 H_2 \quad (9)$$

where H_{sol} is the molar enthalpy of the solution and H_1 and H_2 are the molar enthalpies of the pure components 1 and 2. All enthalpies were calculated by dividing the average potential energy of each system by the total number of molecules in the simulation.

Although the interactions between MSH, MSM, DDS, and water are of interest for potential biomolecular simulations, all three sulfur compounds are sparingly soluble in water. As a result, and since no experimental activity coefficients were available for the aqueous solutions, the simulations and KB analysis were performed using methanol solutions. As a test of the applicability of the KBFF models to aqueous solutions, a simulation was subsequently performed to determine the approximate solubility of MSM in SPC/E water at 300 K. A random initial configuration of 1018 MSM and 4178 SPC/E water molecules (volume fraction of 0.5) was arranged in a rectangular box with dimensions of 5 nm × 5 nm × 10 nm. The energy of the system was minimized using 10 000 steps of steepest descent. The system was then allowed to equilibrate for 200 ps. During this time, the system almost completely phase separated. A 20 ns production run was then performed. The solubility of MSM in water was calculated by fitting the density profile of MSM along the extended simulation box dimension, $\rho(z)$, to the hyperbolic tangent function[30]

$$\rho(z) = \frac{1}{2}(\rho_{MSM,l} + \rho_{MSM,aq}) - \frac{1}{2}(\rho_{MSM,l} - \rho_{MSM,aq})\tanh[(z - z_0)/d] \quad (10)$$

where $\rho_{MSM,l}$ is the bulk density of MSM; $\rho_{MSM,aq}$ is the density of MSM in water; z_0 is the location of the MSM/water interface; and d is the width of the interface. The fitting was repeated in 2.5 ns blocks, and the concentration of MSM in water was determined as a function of simulation time.

Kirkwood−Buff Analysis of Simulation Data. The chemical potential derivatives, D, were obtained from the simulations via the Kirkwood−Buff (KB) integrals defined in eq 1. Although the direct evaluation of the integrals in eq 1 is practically impossible, since it would require very large simulations in the grand canonical ensemble, it can been shown that G_{ij} can be approximated by[11]

$$G_{ij} = 4\pi \int_0^{R_c} [g_{ij}^{NpT}(r) - 1] r^2 dr \quad (11)$$

where g_{ij}^{NpT} is the radial distribution function between molecules i and j in the NpT ensemble and R_c is the cutoff distance at which the radial distribution function is considered to be unity. In practice, the KB integrals are calculated and averaged over a small range of distances to eliminate small fluctuations in their values. In this work, that distance was between 2.0 and 2.5 nm. A series of KB integral values were determined from 1.25 ns ensemble averages, thereby providing an estimate of the standard deviation from the mean. Using the KB integrals from simulations, the activity derivative can be expressed as[6]

$$\frac{\partial \ln \gamma_1}{\partial \ln x_1} = \frac{-x_1 \rho_2 \Delta G}{1 + x_1 \rho_2 \Delta G} \quad (12)$$

where $\Delta G = G_{11} + G_{22} - 2G_{12}$, and therefore the chemical potential derivative D from eq 5 can be calculated. The partial molar volume of each component as a function of mole fraction was obtained directly from the simulated KB integrals[6]

$$\overline{V_1} = \frac{1 + \rho_2(G_{22} - G_{12})}{\rho_1 + \rho_2 + \rho_1 \rho_2 \Delta G} \quad (13)$$

$$\overline{V_2} = \frac{1 + \rho_1(G_{11} - G_{12})}{\rho_1 + \rho_2 + \rho_1 \rho_2 \Delta G} \quad (14)$$

To determine the parameters of the Wilson equation which best represent the simulated data, the sum of the activity derivatives obtained from our simulations was determined

$$\frac{\partial \ln \gamma_1}{\partial \ln x_1} + \frac{\partial \ln \gamma_2}{\partial \ln x_2} = 2\frac{-x_1 \rho_2 \Delta G}{1 + x_1 \rho_2 \Delta G} \quad (15)$$

and then fitted to the corresponding expression obtained from the Wilson equation

$$\frac{\partial \ln \gamma_1}{\partial \ln x_1} + \frac{\partial \ln \gamma_2}{\partial \ln x_2} = -\frac{x_1 - \Lambda_{12}x_2}{x_1 + \Lambda_{12}x_2} - \frac{x_2 - \Lambda_{21}x_1}{x_2 + \Lambda_{21}x_1} - 2x_1x_2\left[\frac{\Lambda_{12}(1 - \Lambda_{12})}{(x_1 + \Lambda_{12}x_2)^2} + \frac{\Lambda_{21}(1 - \Lambda_{21})}{(x_2 + \Lambda_{21}x_1)^2}\right] \quad (16)$$

This approach helps to bias the fit toward the activity derivative with the most statistical significance, i.e., d ln γ_i as x_j tends to zero.

Development of Force Field Parameters. The Kirkwood−Buff derived force field used in this study is comprised of a Lennard-Jones (LJ) 6-12 and a Coulombic potential. The combination rules used for the LJ parameters were $\varepsilon_{ij} = (\varepsilon_{ii}\varepsilon_{jj})^{1/2}$ and $\sigma_{ij} = (\sigma_{ii}\sigma_{jj})^{1/2}$. Table 3 shows the final parameters used in our simulations. The LJ parameters for hydrogen and oxygen atoms were taken from Weerasinghe and Smith,[6] and the united atom methyl group parameters used for all molecules were taken from Daura et al.[31] The KBFF models have been developed with the philosophy that the number of atom types is kept to a minimum. New atom types are generally only adopted when there is a change in hybridization of an atom. Hence, only one atom type was assumed for all the sulfur molecules investigated here. The LJ parameters for sulfur in MSH and MSM were set equal to each other and varied until they reproduced, as closely as possible, the experimental densities of pure MSH and MSM. This approach for determining the LJ parameters differed from the simple scheme[7] used for the KBFF model of methanol and other solutes.[6] The previous approach did not work for the sulfur compounds studied here, probably because sulfur is the first third row atom investigated. The optimal values of the LJ parameters determined here are the same as those previously used by Lubna et al.[20] for the sulfur in MSH. The same LJ parameters were then used for the sulfur in DDS. The force field for MOH was taken from Weerasinghe and Smith,[6] and the charges on the other three solute molecules were optimized so that they best reproduced the variation in excess coordination numbers for mixtures of the solutes with methanol across the whole mole fraction range. Approximately 30 charge distributions were tested.

The molecular geometries used in our simulations are presented in Table 4. The geometry for MOH was taken from Weerasinghe and Smith,[6] and the geometries of the sulfur compounds were taken from Lubna et al.[20] Only DDS contains a dihedral angle conformational degree of freedom. The energy as a function of the CH−S−S−CH dihedral angle in DDS was calculated using Gaussian ′03[32] at the b3lyp/6-311g++ level of theory. A torsional potential corresponding to $V = 5.8[1 + \cos \phi] + 17.5[1 + \cos 2\phi] + 4.2[1 + \cos 3\phi]$, as a function of the CH−S−S−CH dihedral angle (ϕ), was then determined from a fit to the gas phase rotational energy surface.

Results

Using the approaches described in the Methods section, a series of charge distributions for the above molecules were investigated and the resulting properties of their mixtures with MOH determined. The simulated KB integrals varied significantly depending on the charge distribution used. This type of sensitivity of the KB integrals to the effective charge distribution is in agreement with our previous studies and, in our opinion, a major advantage of the current approach. The majority of the trial charge distributions resulted in excessive aggregation of the solute molecules and therefore an incorrect balance of solute−solute and solute−solvent interactions, which was characterized by large positive N_{22} (and N_{11}) values significantly in excess of the experimental values. The last column of Table 3 indicates the best charge distributions obtained for MSH, MSM, and DDS determined in the present study. The difference between the absolute charge on sulfur and that on hydrogen in MSH (0.56 e), in comparison to that between oxygen and hydrogen in MOH (1.34 e), suggests that hydrogen bonding is far less likely between molecules of MSH compared to molecules of MOH.

Figure 1 displays the final excess coordination numbers for MSM/MOH solutions as a function of the MSM mole fraction. In comparison, the filled circles correspond to the excess coordination numbers predicted by the combination of the MSM force field developed by Lubna et al.[20] with the KBFF force field for MOH developed by Weerasinghe and Smith.[6] Although we also performed simulations with the Lubna et al. and KBFF MOH force field across the entire mole fraction range, only three data points are shown in Figure 1 for simplicity. The predictions deviate significantly from experiment. This clearly indicates that the Lubna et al.[20] force field is incompatible with our KBFF model for MOH. A similar incompatibility between the two force fields was also observed for the other solutes studied in this work, but the results are not shown on the respective figures for clarity of presentation. This emphasizes that one cannot simply combine existing force fields, developed using different approaches, and expect the mixture properties to be accurately reproduced.

The open circles in Figure 1 correspond to the excess coordination numbers predicted by the combination of the MSM force field developed in this work with the KBFF model for

TABLE 3: Final Nonbonded Force Field Parameters for the KBFF Models[a]

molecule	atom	ε, kJ/mol	σ, nm	q
methane thiol	S	1.6545	0.3580	−0.44
	H	0.0880	0.1580	+0.12
	CH	0.8672	0.3748	+0.32
dimethyl sulfide	S	1.6545	0.3580	−0.44
	CH	0.8672	0.3748	+0.22
dimethyl disulfide	S	1.6545	0.3580	−0.31
	CH	0.8672	0.3748	+0.31
methanol[b]	O	0.6506	0.3192	−0.82
	H	0.0880	0.1580	+0.52
	CH	0.8672	0.3748	+0.30

[a] The combination rules used for ε and σ were $\varepsilon_{ij} = (\varepsilon_{ii}\varepsilon_{jj})^{1/2}$ and $\sigma_{ij} = (\sigma_{ii}\sigma_{jj})^{1/2}$. [b] The force field of methanol was taken from Weerasinghe and Smith.[6]

TABLE 4: Bonded Force Field Parameters for the KBFF Models[a]

molecule	bond	nm	angle, θ	deg
methane thiol[b]	S−H	0.134	CH−S−H	96
	S−CH	0.182		
dimethyl sulfide[b]	S−CH	0.182	CH−S−CH	99
dimethyl disulfide[b]	S−S	0.204	CH−S−S	103.7
	S−CH	0.181		
methanol[c]	O−H	0.0945	CH−O−H	108.5
	O−CH	0.143		

[a] For DDS, the rotational potential is $5.8[1 + \cos \phi] + 17.5[1 + \cos 2\phi] + 4.2[1 + \cos 3\phi]$, where ϕ is the CH−S−S−CH dihedral angle. Also, the 1−4 interactions were removed and the harmonic angle potential had the form $(1/2)k(\theta - \theta_0)^2$, where θ is the CH−S−S angle in radians and $k = 5690.24$ kJ/mol. [b] The initial geometries of methane thiol, dimethyl sulfide, and dimethyl disulfide were taken from Lubna et al.[20] [c] The initial geometry of methanol was taken from Weerasinghe and Smith.[6]

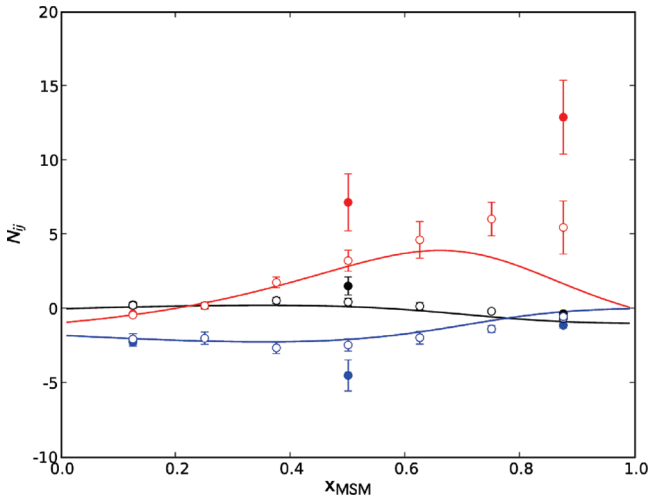

Figure 1. Excess coordination numbers for dimethyl sulfide/methanol (MSM/MOH) solutions as a function of the MSM mole fraction at 288 K. Solid lines correspond to our analysis of the experimental data,[16] open circles to simulation data based on the KBFF model, and closed circles to simulation data based on the Lubna et al.[20] force field for MSM. Black lines and circles correspond to MSM/MSM, red to MOH/MOH, and blue to MSM/MOH pairs.

MOH developed by Weerasinghe and Smith.[6] Although the approach used here for developing the LJ parameters for sulfur (variation of the LJ parameters until the experimental densities of pure MSH and MSM were reproduced) was different from the simple scheme[7] used previously by Weerasinghe and Smith for the MOH force field,[6] the combined models quantitatively predict the experimental MSM/MSM and MSM/MOH excess coordination numbers across the entire mole fraction range. Although the KBFF results deviate slightly from experiment for the MOH/MOH coordination numbers at high MSM mole fractions, this can probably be attributed to an increased uncertainty in the determination of the excess coordination numbers, by either simulation or experiment, at such mole fractions.

Figure 2 shows the molecule-based radial distribution functions (rdf) for equimolar solutions of MSH/MOH, MSM/MOH, and DDS/MOH. All rdfs approach unity beyond 1.2 nm or so. The first shell coordination numbers for all four systems were calculated from the corresponding rdfs and are presented in the Supporting Information. The first shell coordination numbers decreased monotonically from their values for the pure substances, which were 12.4 at 0.648 nm for MSH, 12.6 at 0.718 nm for MSM, and 12.8 at 0.763 nm for DDS. The large first shell coordination numbers for the sulfur molecules is a direct consequence of the rather large spatial extent of the solvation shells, especially in comparison with MOH.

Figure 3 indicates the excess coordination numbers for MSH/MOH solutions as a function of the mole fraction of MSH. The KBFF model quantitatively reproduces the experimental data, although predicted errors are again high at large mole fractions of MSH. A similar quantitative agreement between the KBFF model and experiment appears in Figure 4 for the variation of the excess coordination numbers in DDS/MOH solutions as a function of the DDS mole fraction. It is interesting to note that in both the MSM/MOH and the DDS/MOH systems only one parameter, the charge on sulfur, was adjusted for the simulations to agree with experiment.

Figure 5 displays the excess coordination numbers for the MSH/MSM solutions as a function of the MSH mole fraction. The agreement between the KBFF model and experiment is

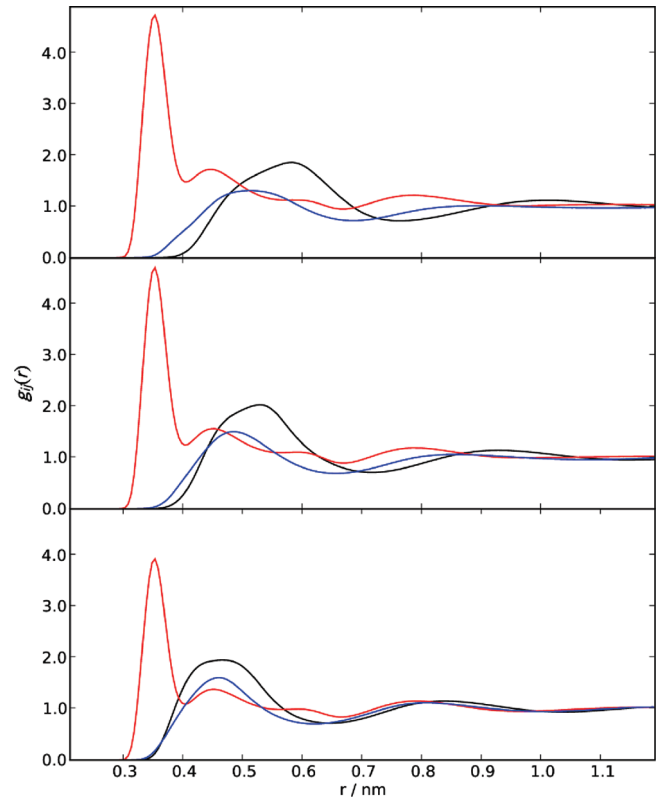

Figure 2. Radial distribution functions for equimolar solutions of methanethiol/methanol (MSH/MOH), dimethyl sulfide/methanol (MSM/MOH), and dimethyl disulfide/methanol (DDS/MOH) as a function of distance. Top panel corresponds to a solution of MSH/MOH at 288 K, middle to MSM/MOH at 288 K, and bottom to DDS/MOH at 311 K. Black lines and symbols correspond to MSH/MSH, MSM/MSM, or DDS/DDS; red to MOH/MOH; blue to MSH/MOH, MSM/MOH, or DDS/MOH pairs.

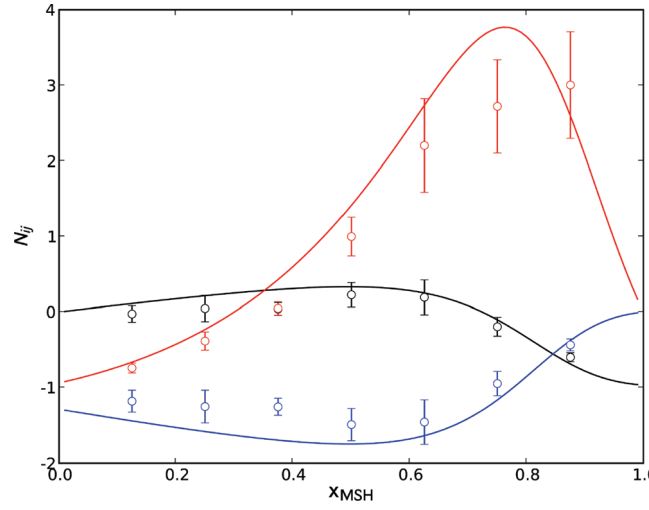

Figure 3. Excess coordination numbers for methanethiol/methanol (MSH/MOH) solutions as a function of the MSH mole fraction at 288 K. Solid lines correspond to our analysis of the experimental data[16] and open circles to simulation data based on the KBFF model. Black lines and circles correspond to MSH/MSH, red to MOH/MOH, and blue to MSH/MOH pairs.

excellent. It is important to note that none of the parameters of MSH or MSM were adjusted to achieve the agreement shown in Figure 5. The MSH/MSM mixture provides a rare example of an (almost) ideal solution over the full composition range. For symmetric ideal (SI) solutions, the excess coordination numbers depend only on the properties of the pure components.[11]

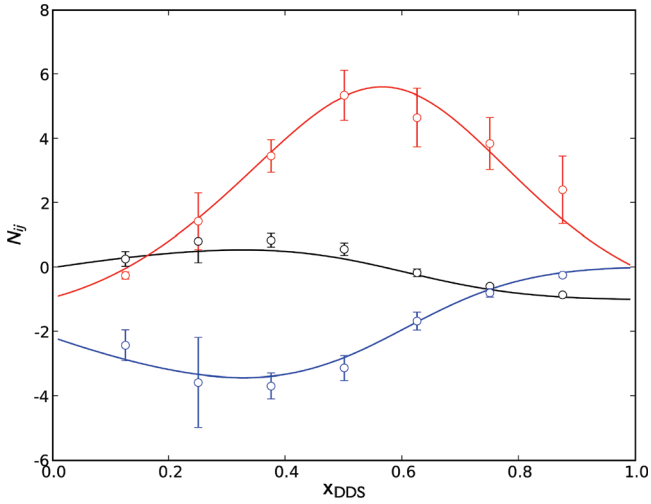

Figure 4. Excess coordination numbers for dimethyl disulfide/methanol (DDS/MOH) solutions as a function of the DDS mole fraction at 311 K. Solid lines correspond to our analysis of the experimental data[17] and open circles to simulation data based on the KBFF model. Black lines and circles correspond to DDS/DDS, red to MOH/MOH, and blue to DDS/MOH pairs.

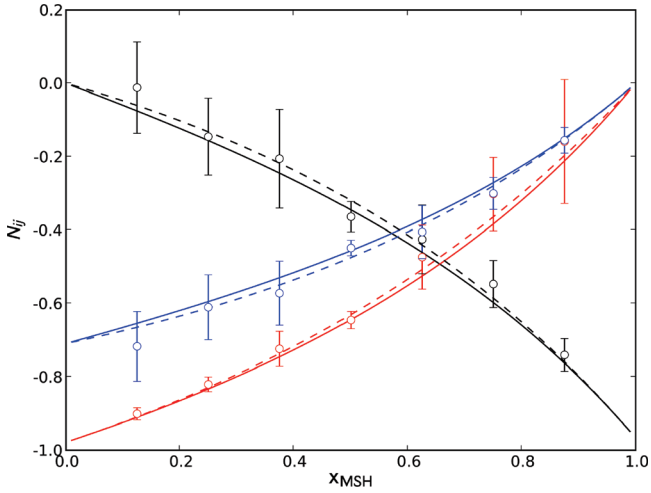

Figure 5. Excess coordination numbers for methanethiol/dimethyl sulfide (MSH/MSM) solutions as a function of the MSH mole fraction at 288 K. Solid lines correspond to our analysis of the experimental data[16] and open circles to simulation data based on the KBFF model. The dashed lines correspond to the results expected for a symmetric ideal solution for which[11,22] $G_{ij}^{SI} = RT\kappa_T - V_i - V_j + \rho_1 V_1^2 + \rho_2 V_2^2$ and where we have taken $V_1 = V_{MSH} = 54$ cm^3·mol^{-1} and $V_2 = V_{MSM} = 74$ cm^3·mol^{-1}. Black lines and circles correspond to MSH/MSH, red to MSM/MSM, and blue to MSH/MSM pairs.

Ideal behavior is illustrated by the dashed lines in Figure 5. The SI behavior of the solution is also apparent in the rdfs obtained for MSH/MSH, MSM/MSM, and MSH/MSM pairs as a function of MSH mole fraction displayed in Figure 6. The three rdfs are remarkably independent of composition and can be superimposed up to a distance of 1.1 nm, where a minute difference between the curves can be detected. Furthermore, the almost identical features of the rdfs, except for the slight shift in distance, are noticeable. This ideal behavior is somewhat unexpected for two reasons. First, one could argue that MSH would be a potential hydrogen bond donor and acceptor, whereas MSM would only be a hydrogen bond acceptor. Second, although the charge on the sulfur in both molecules is the same (−0.44 *e*), the difference in the molar volumes between MSH and MSM is such that ideal solution would not be obvious.

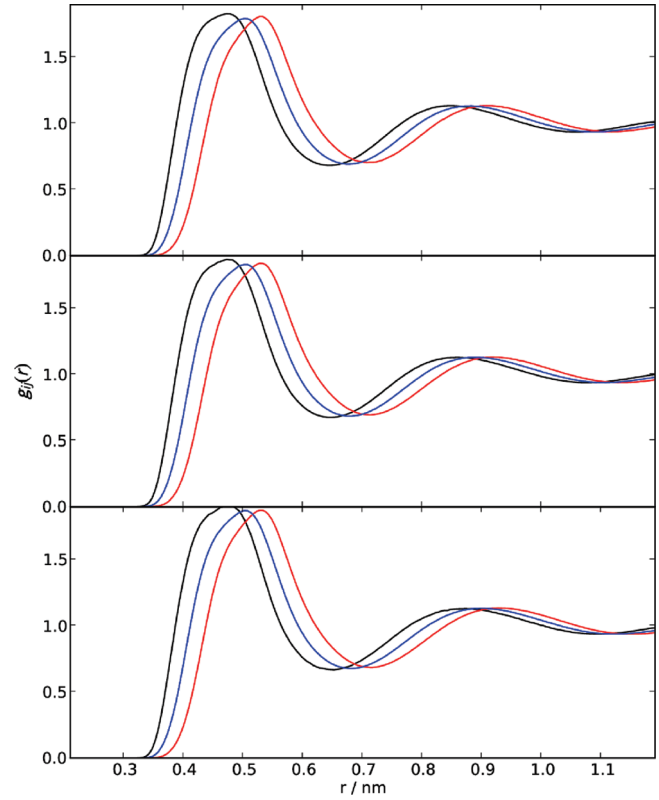

Figure 6. Radial distribution functions for three methanethiol/dimethyl sulfide (MSH/MSM) solutions as a function of distance at 288 K. The top panel corresponds to MSH mole fractions of 0.25, middle to 0.50, and bottom to 0.75. Black lines and symbols correspond to MSH/MSH, red to MSM/MSM, and blue to MSH/MSM pairs.

Clearly, this is not the case here, and so one must conclude that the similar charge distributions used for both models dominate the solution properties, even though both molecules have somewhat different sizes.

Table 1 provides the parameters Λ_{12} and Λ_{21} of the Wilson equation for the experimental data[16,17] and determined from the simulated KBIs using the KBFF models. Although the simulated and experimental values of Λ_{12} and Λ_{21} are similar for three of the four solutions (MSM/MOH, MSH/MSM, and DDS/MOH), they differ significantly for the MSH/MOH solution. This is probably due to the large uncertainties in the evaluation of the Kirkwood-Buff integrals at large mole fractions of MSH (see discussion of Figure 3). The values of Λ_{12} and Λ_{21} for the MSH/MSM solution are very close to unity. This indicates that the left-hand side of eqs 6 and 7 approaches zero, and therefore γ_1 and γ_2 approach unity, which is indicative of an ideal solution.

Figure 7 displays the excess enthalpy of mixing for the various solutions as a function of composition. Three of the four solutions display deviations from ideal solution behavior with the deviations being the largest for the DDS/MOH solution. The excess enthalpies of mixing for MSH/MOH and MSM/MOH mixtures are both positive and almost identical. This can be explained by the similarity between the final charge distributions for the MSH and MSM molecules and the close to ideal thermodynamics observed for their mixture. For the MSH/MSM solutions, the excess enthalpy is very close to zero for all mole fractions, again indicating the ideality of the solution. Figure 8 shows the self-diffusion constants for each component of the four solutions studied in this work. They all exhibit an essentially linear variation with mole fraction. The diffusion constants for both components increase as a function of mole fraction for the MSH/MOH and the MSM/MOH solutions, but they decrease

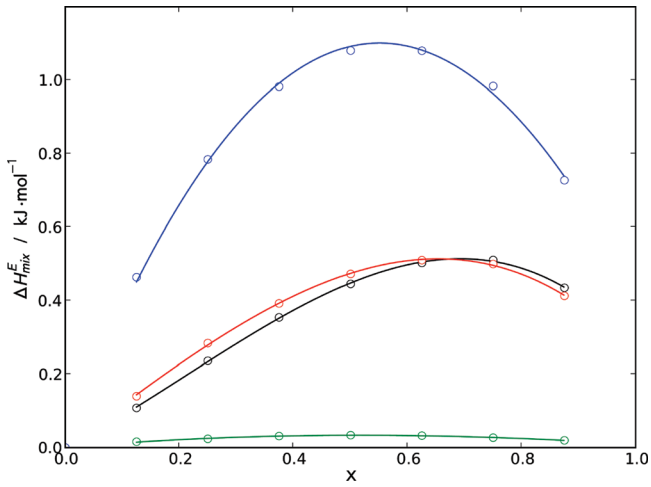

Figure 7. Excess enthalpy of solution as a function of mole fraction obtained from the simulation data using the KBFF models. Black circles correspond to methanethiol/methanol solutions at 288 K, red to dimethyl sulfide/methanol solutions at 288 K, green to methanethiol/dimethyl sulfide solutions at 288 K, and blue to dimethyl disulfide/methanol solutions at 311 K. The solid lines are drawn to guide the eye.

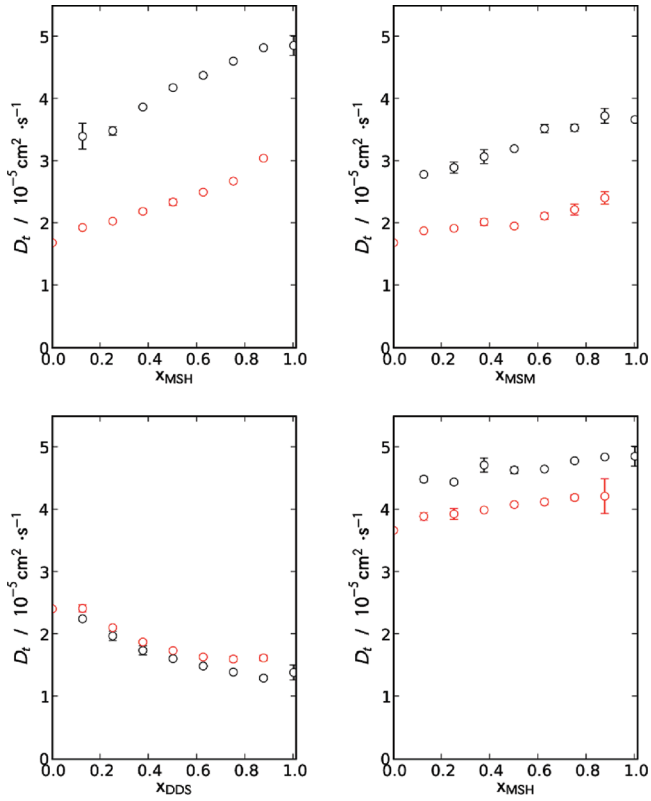

Figure 8. Self-diffusion constants of the solution components as a function of composition obtained from the simulation data using the KBFF models. Upper-left panel: solutions of methanethiol/methanol (MSH/MOH) at 288 K, where black circles correspond to MSH and red to MOH. Upper-right panel: solutions of dimethyl disulfide/methanol (DDS/MOH) at 311 K, where black circles correspond to DDS and red to MOH. Lower-right panel: solutions of dimethyl sulfide/methanol (MSM/MOH) at 288 K, where black circles correspond to MSM and red to MOH. Lower-left panel: solutions of methanethiol/dimethyl sulfide (MSH/MSM) at 288 K, where black circles correspond to MSH and red to MSM.

for the DDS/MOH solution. In addition, the diffusion constants do not vary appreciably with mole fraction for the MSH/MSM system, a further observation that is consistent with MSH and MSM forming an ideal solution.

TABLE 5: Experimental and Simulated Density, ρ, Dielectric Constant, ε, Thermal Expansion Coefficient, α, Heat Capacity, C_p, Isothermal Compressibility, κ_T, and Self-Diffusion Constant, D_t, at 1 atm and 298 K for the Molecules Studied in This Work

molecule	property	experiment	simulation	units
methane thiol	ρ	0.862[a]	0.893	g cm^{-3}
	η	0.25[a]	0.30	10^{-3} kg m s^{-1}
	α	1.59[a]	1.5	10^{-3} K^{-1}
	κ_T		7.6	10^{-5} atm^{-1}
	D_t	<6.5[b]	4.9	10^{-5} cm^2 s^{-1}
	ε		20	
	C_p	96.4[a]	71.3	J mol^{-1} K^{-1}
dimethyl sulfide	ρ	0.848[a]	0.863	g cm^{-3}
	η	0.28[a]	0.33	10^{-3} kg m s^{-1}
	α	1.42[a]	1.2	10^{-3} K^{-1}
	κ_T		6.8	10^{-5} atm^{-1}
	D_t		3.7	10^{-5} cm^2 s^{-1}
	ε	6.70[c]	13	
	C_p	122[a]	75.1	J mol^{-1} K^{-1}
dimethyl disulfide	ρ	1.06[a]	1.120	g cm^{-3}
	η	0.57[a]	0.91	10^{-3} kg m s^{-1}
	α	1.05[a]	0.9	10^{-3} K^{-1}
	κ_T		4.5	10^{-5} atm^{-1}
	D_t		1.4	10^{-5} cm^2 s^{-1}
	ε	9.6[c]	17	
	C_p	148[a]	112	J mol^{-1} K^{-1}
methanol[d]	ρ	0.786	0.763	g cm^{-3}
	η	0.54	0.45	10^{-3} kg m s^{-1}
	α	1.2	1.2	10^{-3} K^{-1}
	κ_T	12.1	10.4	10^{-5} atm^{-1}
	D_t	2.42	2.1	10^{-5} cm^2 s^{-1}
	ε	32.3	36	
	C_p	80	86[e]	J mol^{-1} K^{-1}

[a] Experimental data from Yaws.[25] [b] Experimental data from Sampson and Carpenter.[33] [c] Experimental data from Lide.[38] [d] Experimental and simulation data from Weerasinghe and Smith.[6] [e] The heat capacity of methanol reported by Weerasinghe and Smith[6] has been corrected for quantum effects.

Table 5 shows the experimental and simulated density, ρ, shear viscosity, η, dielectric constant, ε, thermal expansion coefficient, α, heat capacity, C_p, isothermal compressibility, κ_T, and self-diffusion constant, D_t, at 1 atm and 298 K for the pure substances studied in this work. The densities, dielectric constants, and self-diffusion constants for all four solutions studied in this work can be found in the Supporting Information. Although the LJ parameters for sulfur were chosen to minimize the sum of the deviations between the simulated and experimental densities for both MSH and MSM, they do not predict both of the densities exactly. In addition, the KBFF model underestimates the density of DDS by 0.06 g/cm, since the LJ parameters for sulfur in DDS were assumed to be the same as those in MSH and MSM. It is our intention to keep the number of atom types used in our force fields to a minimum. Consequently, some of these deviations are unavoidable. The simulated shear viscosities were close to the experimental values for MSH and MSM but less accurate for DDS. The thermal expansion coefficients for MSH, MSM, and DDS were close to those determined by experiment. Unfortunately, there was no experimental data available for the isothermal compressibilities. Experimental data were also not available for the self-diffusion constants of MSM and DDS, but the simulated value for pure MSH was in accord with an upper bound determined by neutron scattering.[33] The simulated dielectric constants of MSM and DDS were slightly high, while no experimental dielectric constant was available for MSH. The simulated heat capacities of MSH, MSM, and DDS were lower than those determined

experimentally. This is due to the fact that the molecules in our simulations were not allowed to vibrate and because the required quantum corrections were unavailable.[34] In general, the small disagreements between simulation and experiment can be explained by the following two reasons. First, the KBFF models have a limited number of atom types: only one type of sulfur for MSH, MSM, and DDS, and one type of hydrogen for MOH and MSH. Second, the KBFF models have been developed to reproduce the solution properties of mixtures and have not focused on generating very accurate properties of pure liquids.

As mentioned previously, we were forced to study mixtures with methanol due to the low solubility of the solutes in water. Our main assumption is that if one has, for example, the correct properties for MOH/HOH mixtures and MSM/MOH mixtures then one can have some confidence in the resulting interactions obtained between MSM and HOH molecules. The validity of this assumption is difficult to prove. The sulfur compounds are hydrophobic in nature, hence their low solubility in water. Methanol represents a polar solvent which, although not as polar as water, provides some confidence that mixtures of our sulfur models with water will behave correctly. Alternatively, many researchers use free energies of solvation or enthalpies of vaporization to validate or develop force field parameters. We have refrained from doing this here for the simple reason that these measures involve corrections to account for condensed phase polarization effects and quantum corrections to vibrational frequencies, for them to be useful. In many cases, these additional data are not known. Consequently, as the KBFF models have been developed to mimic these condensed phase effects a fair comparison with experiment is only possible in limited cases. Our model for pure methanol was one of these cases and provided an excellent value for the enthalpy of vaporization.[6]

However, the low solubility of MSM in water is known. Therefore, we decided to determine the solubility of our MSM model in water as an initial test of the above assumption. The top panel of Figure 9 indicates the resulting density profiles for water and MSM at 298 K approximately 9 ns after the initial phase separation. The immiscibility of MSM with water was clearly reproduced. Fitting the density profile at different simulation times to eq 10, the solubility of MSM in the water-rich region was determined and is displayed in the bottom panel of Figure 9. The calculated solubility of MSM in water appears to stabilize at $6(1) \times 10^3$ ppm after 10 ns of simulation time, a value that is similar to the experimentally determined value of approximately 20×10^3 ppm.[25] This result seems reasonable considering the relatively few MSM molecules observed in the water-rich region.

All three solutes display a maximum in the experimental methanol−methanol KB integrals (N_{11}) as the methanol mole fraction decreases. This indicates a significant increase in the self-association of methanol molecules at these compositions. This type of behavior is illustrated in the oxygen−oxygen rdfs for the MSH/MOH, MSM/MOH, and DDS/MOH solutions as shown in Figure 10. A large first solvation shell of methanol around methanol develops as the methanol mole fraction decreases. However, the corresponding first shell coordination numbers for the oxygen atoms are also shown in Figure 10 and do not exhibit any maxima. In particular, all the oxygen−oxygen first shell coordination numbers decrease monotonically from their value of ≈ 2, which corresponds to pure MOH. The high value for the first peak in the rdfs at low MOH concentrations suggests the existence of methanol aggregates. Further examination of the configurations generated for the MSH/MOH mixture at $x_{MSH} = 0.875$ indicates that this is indeed the case. Some representative structures are displayed in Figure 11. Hydrogen-bonded chains and cyclic clusters are clearly observed. These types of structures are similar to the gas-phase methanol clusters that have been observed by X-ray diffraction[35,36] and X-ray emission spectroscopy.[37]

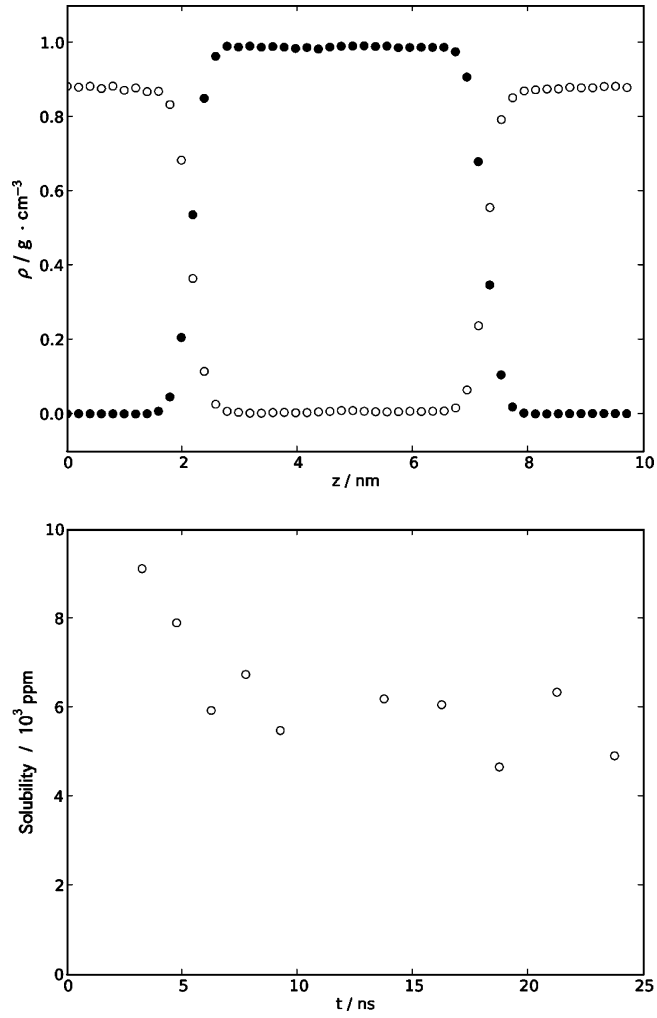

Figure 9. Top panel: Density profiles for the dimethyl sulfide/water system at 298 K obtained from the simulation ≈ 9 ns after phase separation. Open circles correspond to the density of dimethyl sulfide and filled circles to the density of water. Bottom panel: the variation of the solubility of dimethyl sulfide in the water-rich region as a function of simulation time after the initial major phase separation.

Conclusions

KB derived force fields for MSH, MSM, and DDS have been generated using experimental information concerning the activity of these solutes in MOH solutions. The KBFF models quantitatively reproduce the experimental excess coordination numbers of MSH/MOH, MSM/MOH, and DDS/MOH solution mixtures. In addition, the KBFF models also quantitatively predicted the excess coordination numbers of MSH/MSM solutions, data that were not used during the parametrization. The KBFF force fields provide reasonable agreement with experiment for the properties of the pure substances and therefore reliable estimates for the excess enthalpy of mixing of the solutions and the self-diffusion constants of the substances in solution, where experimental data are not available. The KBFF model for MSM reproduced the fact that MSM and water mixtures should phase separate, and

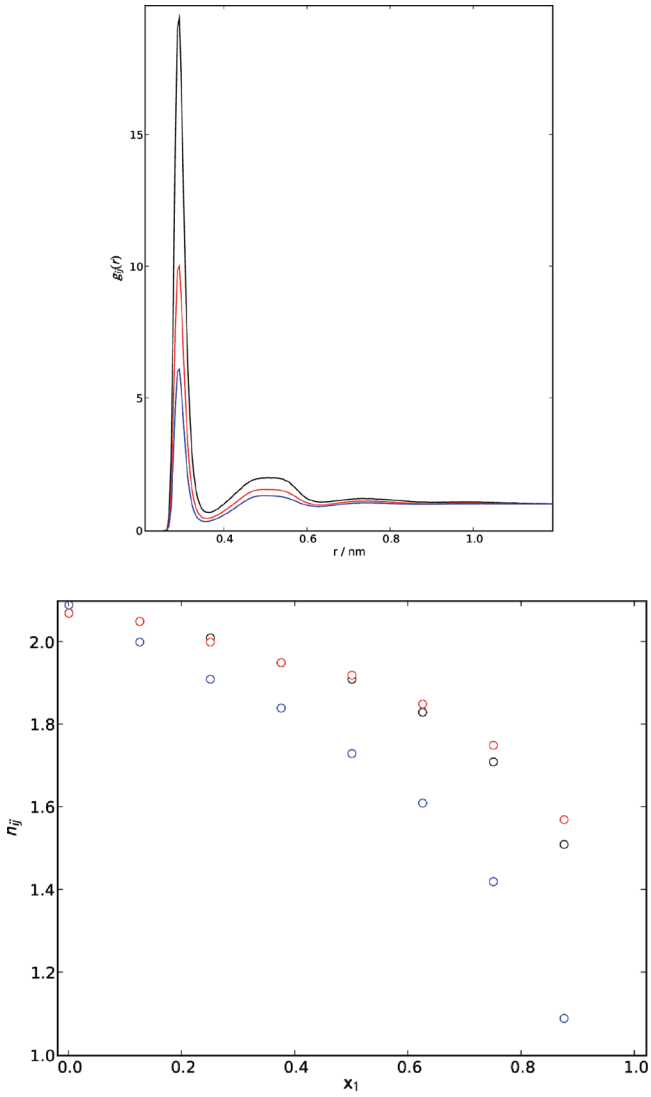

Figure 10. Top panel: Oxygen−oxygen radial distribution functions in three different MSM/MOH solutions. Black line corresponds to 0.25, red to 0.5, and blue to 0.75 mol fractions of MSM. Bottom panel: Oxygen−oxygen first shell coordination numbers from simulation data obtained for the KBFF models as a function of the mole fraction x_1, where 1 corresponds to MSH, MSM, and DDS in MSH/MOH, MSM/MOH, and DDS/MOH solutions, respectively. Black circles correspond to the MSH/MOH, red to the MSM/MOH, and blue to the DDS/MOH solution.

a reasonable value for the solubility of MSM in water was obtained. Therefore, we have high confidence that the above models provide reasonable balanced descriptions of the interactions of these molecules in MOH (and water) solutions. The use of the KB integrals during the parametrization procedure highlights a particular advantage of this approach for systems where there is limited experimental data on diffusion constants, dielectric constants, enthalpy of mixing, etc. Without the KB integrals, it would be very difficult to validate these force fields.

A possible limitation of the KBFF models presented here is that, because they were developed and tested for temperatures near 300 K, applications at higher temperatures may be problematic. In particular, at higher temperatures the volumetric properties of the pure substances will undoubtedly compare unfavorably in comparison with the Delhommelle et al.[19] or the Lubna et al.[20] force fields. However, as biomolecules are the main perceived applications of the new models, this is a relatively minor issue which should not affect simulations at reasonable temperatures.

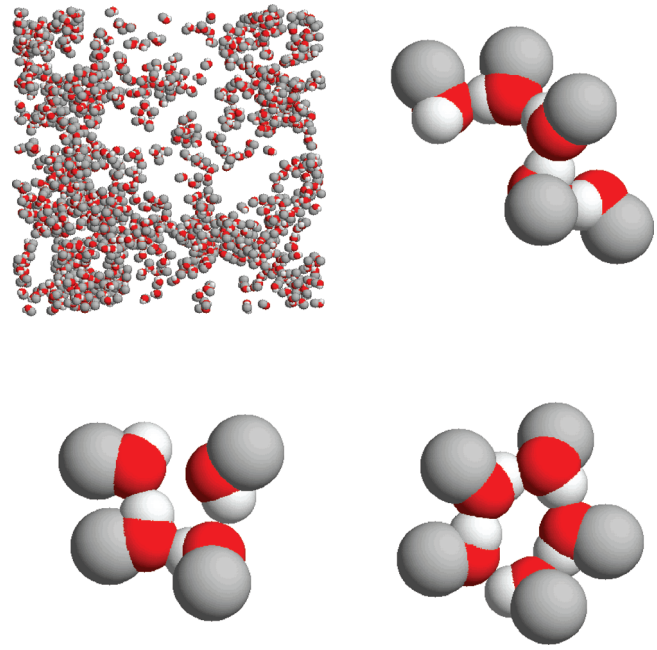

Figure 11. Snapshots of MOH configurations from the MSH/MOH mixture at $x_{MSH} = 0.875$. The MSH molecules have been omitted for clarity. Upper-left: a snapshot from the simulation indicating significant aggregation of MOH molecules. Upper-right: a MOH pentamer chain. Lower-left: an almost ideal MOH tetramer. Lower-right: a MOH pentamer.

Acknowledgment. The project described was supported by Grant Number R01GM079277 (PES) from the National Institute of General Medical Sciences. The content is solely the responsibility of the authors and does not necessarily represent the official views of the National Institute of General Medical Sciences or the National Institutes of Health. N.B. and N.R.C. would like to acknowledge the financial support of the Welch Foundation and of Southwestern University.

Supporting Information Available: Values of the density, diffusion constants, relative permittivities, and first-shell coordination numbers as a function of composition for all the mixtures studied here are provided. This material is available free of charge via the Internet at http://pubs.acs.org.

References and Notes

(1) Brooks, B. R.; Bruccoleri, R. E.; Olafson, B. D.; States, D. J.; Swaminathan, S.; Karplus, M. *J. Comput. Chem.* **1983**, *4*, 187–217.
(2) Cornell, W. D.; Cieplak, P.; Bayly, C. I.; Gould, I. R.; Merz, K. M.; Ferguson, D. M.; Spellmeyer, D. C.; Fox, T.; Caldwell, J. W.; Kollman, P. A. *J. Am. Chem. Soc.* **1995**, *117*, 5179–5197.
(3) Damm, W.; Frontera, A.; Tirado-Rives, J.; Jorgensen, W. L. *J. Comput. Chem.* **1997**, *18*, 1955–1970.
(4) van Gunsteren, W. F. *Biomolecular Simulation: The Gromos96 Manual und User Guide*; vdf Hochschulverlag ETH: Zurich, 1996.
(5) Kang, M.; Smith, P. E. *J. Comput. Chem.* **2006**, *27*, 1477–1485.
(6) Weerasinghe, S.; Smith, P. E. *J. Phys. Chem. B* **2005**, *109*, 15080–15086.
(7) Weerasinghe, S.; Smith, P. E. *J. Phys. Chem. B* **2003**, *107*, 3891–3898.
(8) Weerasinghe, S.; Smith, P. E. *J. Chem. Phys.* **2003**, *119*, 11342–11349.
(9) Weerasinghe, S.; Smith, P. E. *J. Chem. Phys.* **2004**, *121*, 2180–2186.
(10) Weerasinghe, S.; Smith, P. E. *J. Chem. Phys.* **2003**, *118*, 10663–10670.

(11) Ben-Naim, A. *Molecular Theory of Solutions*; Oxford University Press: USA, 2006.

(12) Pierce, V.; Kang, M.; Aburi, M.; Weerasinghe, S.; Smith, P. E. *Cell Biochem. Biophys.* **2008**, *50*, 1–22.

(13) Weerasinghe, S.; Gee, M. B.; Kang, M.; Bentenitis, N.; Smith, P. E. In *Modeling Solvent Environments*; Wiley-VCH: Weinheim, 2009; In press.

(14) van der Vegt, N. F. A.; van Gunsteren, W. F. *J. Phys. Chem. B* **2004**, *108*, 1056–1064.

(15) Trzesniak, D.; van der Vegt, N. F. A.; van Gunsteren, W. F. *Phys. Chem. Chem. Phys.* **2004**, *6*, 697.

(16) Jackowski, A. J. *Pol. J. Chem.* **1980**, *54*, 1765–1773.

(17) Zudkevitch, D.; Forman, A. L.; Deatherage, W. G. *AIChE Symp. Ser.* **1990**, *86*, 47–61.

(18) Berendsen, H. J. C.; Grigera, J. R.; Straatsma, T. P. *J. Phys. Chem.* **1987**, *91*, 6269–6271.

(19) Delhommelle, J.; Tschirwitz, C.; Ungerer, P.; Granucci, G.; Millie, P.; Pattou, D.; Fuchs, A. H. *J. Phys. Chem. B* **2000**, *104*, 4745–4753.

(20) Lubna, N.; Kamath, G.; Potoff, J. J.; Rai, N.; Siepmann, J. I. *J. Phys. Chem. B* **2005**, *109*, 24100–24107.

(21) Ben-Naim, A. *J. Chem. Phys.* **1977**, *67*, 4884–4890.

(22) Smith, P. E. *J. Chem. Phys.* **2008**, *129*, 124509–5.

(23) Poling, B. E.; Prausnitz, J. M.; O'Connell, J. *The Properties of Gases and Liquids*, 5th ed.; McGraw-Hill Professional, 2001.

(24) Matteoli, E.; Lepori, L. *J. Chem. Phys.* **1984**, *80*, 2856–2863.

(25) Yaws, C. *Matheson Gas Data Book*, 7th ed.; McGraw-Hill Professional, 2001.

(26) Lindahl, E.; Hess, B.; van der Spoel, D. *J. Mol. Model.* **2001**, *7*, 306–317.

(27) Hess, B.; Bekker, H.; Berendsen, H. J. C.; Fraaije, J. G. E. M. *J. Comput. Chem.* **1997**, *18*, 1463–1472.

(28) Essmann, U.; Perera, L.; Berkowitz, M. L.; Darden, T.; Lee, H.; Pedersen, L. G. *J. Chem. Phys.* **1995**, *103*, 8577–8593.

(29) Palmer, B. J. *Phys. Rev. E* **1994**, *49*, 359.

(30) Alejandre, J.; Tildesley, D. J.; Chapela, G. A. *J. Chem. Phys.* **1995**, *102*, 4574–4583.

(31) Daura, X.; Mark, A. E.; Gunsteren, W. F. V. *J. Comput. Chem.* **1998**, *19*, 535–547.

(32) Frisch, M. J.; Trucks, G. W.; Schlegel, H. B.; Scuseria, G. E.; Robb, M. A.; Cheeseman, J. R.; Montgomery, J.; Vreven, T.; Kudin, K. N.; Burant, J. C.; Millam, J. M.; Iyengar, S. S.; Tomasi, J.; Barone, V.; Mennucci, B.; Cossi, M.; Scalmani, G.; Rega, N.; Petersson, G. A.; Nakatsuji, H.; Hada, M.; Ehara, M.; Toyota, K.; Fukuda, R.; Hasegawa, J.; Ishida, M.; Nakajima, T.; Honda, Y.; Kitao, O.; Nakai, H.; Klene, M.; Li, X.; Knox, J. E.; Hratchian, H. P.; Cross, J. B.; Bakken, V.; Adamo, C.; Jaramillo, J.; Gomperts, R.; Stratmann, R. E.; Yazyev, O.; Austin, A. J.; Cammi, R.; Pomelli, C.; Ochterski, J. W.; Ayala, P. Y.; Morokuma, K.; Voth, G. A.; Salvador, P.; Dannenberg, J. J.; Zakrzewski, V. G.; Dapprich, S.; Daniels, A. D.; Strain, M. C.; Farkas, O.; Malick, D. K.; Rabuck, A. D.; Raghavachari, K.; Foresman, J. B.; Ortiz, J. V.; Cui, Q.; Baboul, A. G.; Clifford, S.; Cioslowski, J.; Stefanov, B. B.; Liu, G.; Liashenko, A.; Piskorz, P.; Komaromi, I.; Martin, R. L.; Fox, D. J.; Keith, T.; Al-Laham, M. A.; Peng, C. Y.; Nanayakkara, A.; Challacombe, M.; Gill, P. M. W.; Johnson, B.; Chen, W.; Wong, M. W.; Gonzalez, C.; Pople, J. A. *Gaussian 03*, revision C.02.

(33) Sampson, T. E.; Carpenter, J. M. *J. Chem. Phys.* **1969**, *51*, 5543–5546.

(34) Berens, P. H.; Mackay, D. H. J.; White, G. M.; Wilson, K. R. *J. Chem. Phys.* **1983**, *79*, 2375–2389.

(35) Magini, M.; Paschina, G.; Piccaluga, G. *J. Chem. Phys.* **1982**, *77*, 2051–2056.

(36) Narten, A. H.; Habenschuss, A. *J. Chem. Phys.* **1984**, *80*, 3387–3391.

(37) Kashtanov, S.; Augustson, A.; Rubensson, J.; Nordgren, J.; Agren, H.; Guo, J.; Luo, Y. *Phys. Rev. B* **2005**, *71*, 104205.

(38) Lide, D. R. *Handbook of Organic Solvents*, 1st ed.; CRC-Press, 1995.

JP904806F